ISSN 1330-3651 (Print), ISSN 1848-6339 (Online) https://doi.org/10.17559/TV-20230703000781
Original scientific paper

Multi-Environment Adaptive Fast Constant False Alarm Detection Algorithm Optimization Strategy

Wei LI*, Qian WANG, Yuan-shuai LAN, Chang-song MA

Abstract: It takes a long time to detect target information in noisy radar information and reduce the probability of false alarm. Therefore, it has become a research direction to reduce the probability of false alarm and the time of effective target detection. This paper introduces a new method to reduce the occurrence of false alarm in non-uniform environment and improve the efficiency of target detection. The proposed method involves a faster and more stable method that involves preprocessing the data set, splitting it into smaller parts, and utilizing a KTH minimum value M determined by an ordered statistics class constant false alarm detection algorithm. Each data point in the small segment is then compared to *M*, anything above *M* is classified as a target, and anything below M is ignored as clutter. Then ESVI-CFAR detection was performed on the selected target to obtain the final detection result. Experimental results show that the proposed method is superior to the traditional VI-CFAR and has better target detection performance.

Keywords: data set; ESVI-CFAR; false alarm probability; noise; VI-CFAR

1 INTRODUCTION

Radar signal detection is one of the key technologies in the field of radar signal application, and it is also the technical basis for searching, locating, tracking and identifying the detected target. In the detection process of radar signals, in order to detect accurate targets, effectively suppress the noise in the background of the detection unit, and improve the detection probability of useful semaphores, statistical false alarm rate and false alarm rate information are essential [1, 2]. However, in radar detector design, the statistics of false alarm rate cannot be accurately determined. In practical applications, the level of CFAR (Constant False Alarm Rate) detection probability (P_d) often determines the performance of the entire system. In addition to the high detection probability, there is also a high false alarm probability [3, 4]. It is mainly manifested in the following aspects: poor anti-interference [5-7]. CFAR relies on the gray level information of image pixels, without considering the spatial correlation information between pixels (such as neighborhood information). Coupled with the existence of external interference, the peaks and troughs of the gray level histogram are not necessarily obvious, so satisfactory segmentation results cannot be obtained. The CFAR algorithm can be optimized for different background noise models, such as Gaussian white noise. However, if the noise model is inaccurate or imperfect, the performance of the algorithm may be affected [8-10]. CFAR algorithm is mainly used to detect target signals in background noise [11]. However, when there are multiple target signals, the algorithm may not be able to distinguish them effectively and handle multi-target scenarios. CFAR algorithm is sensitive to parameter selection [12]. For example, the selection of parameters such as window size and threshold settings may affect the performance of the algorithm. CFAR algorithm needs to perform complex calculations, including calculating the mean value and variance of signal power [13, 14]. Therefore, for large-scale data sets or real-time application scenarios, the algorithm may require a long computation time. Therefore, a variety of faster and more stable target detection methods has been proposed.

2 LITERATURE REVIEW

Johnson and Finn proposed that CA-CFAR (Cell Average-Constant False-Alarm Rate) has good performance in uniform and less targeted environments [15-17], but its performance is seriously degraded in non-uniform environments, especially in clutter edge environments. The probability of false alarm is obviously increased, and there is a serious target masking phenomenon when there are more targets. GO-CFAR (Greatest of Constant False Alarm Rate) proposed by Hansen, although this method has better detection performance at clutter edge [18-21], it can better solve the problem of high false alarm probability at clutter edge. However, it cannot solve the problem of target masking in CA-CFAR with multiple targets. Trunk and Rohlin proposed a new detection method, SO-CFAR (Smallest of Constant False-Alarm Rate), which can reduce the problem of target masking when multiple targets are distributed on one side of the detection unit [22-24]. However, when multiple targets are distributed on both sides of the detection unit, the detection effect decreases obviously and the probability of false alarm is increased. Smith and Varshne proposed the VI-CFAR (Variable Indictor-constant False-Alarm Rate) detector, which integrated the advantages of CA-CFAR, GO-CFAR and SO-CFAR [25-26]. VI-CFAR calculates the second-order statistic VI and the mean ratio of the front and rear sliding Windows MR by referring to the sliding window data, determines whether the sliding window is uniform according to VI, and determines whether the two sides of the detection unit are at the edge of clutter according to MR, and adaptively selects the optimal detection algorithm through the above two judgments. The VI-CFAR detector has a good effect in uniform environment, and also has a good performance in non-uniform condition, but when there is target interference in both front and rear Windows, VI-CFAR still cannot have a good effect. Hao Chengpeng et al proposed the MVI-CFAR (Modified) of OSCA-CFAR (Ordered Statistic and Cell Averaging Constant False Alarm Rate) applied to VI-CFAR Variability Index - Constant False Alarm Rate) algorithm is applied to the detection algorithm of distributed multi-sensors [27]. OSCA-CFAR replaces

the SO-CFAR detector, and when there is target interference in the front and rear Windows, the OSCA-CFAR detector can be used to detect multiple sensors. The results are obviously improved, but OSCA-CFAR not only improves the detection effect, but also increases the probability of false alarm.

The above researches have certain limitations in feature fusion. Most of the algorithms rely on the prior knowledge of experts and are unable to deal with the complex and changeable background and multi-modal targets, and there are serious limitations in the processing of dynamic point clouds. In this paper, based on the existing detector optimization, the ESVI-CFAR detection algorithm is proposed, the Grubbs criterion is used to eliminate errors, and the unit average minimum constant false alarm detection is adopted to greatly reduce the problem of high false alarm probability caused by SO-CFAR. By using the optimized sample and increasing the negative sample, the detection speed is improved, the clutter interference is effectively suppressed, and the false detection rate is reduced.

3 IMPLEMENTATION PRINCIPLE OF ESVI-CFAR DETECTOR

3.1 ESVI-CFAR Detector

Schematic diagram of ESVI-CFAR detector is shown in Fig. 1. *D* is the detection unit, *P* is the protection unit, X_n is the reference unit. The reference unit X_n is distributed on both sides of the detection unit and the protection unit. VI represents the statistical variance, SUM represents the sum of X_n reference units, and then the statistical mean ratio of the front and rear sliding Windows is calculated. The VI value implies whether the unilateral reference unit is evenly distributed, and the MR Value implies whether there is clutter edge in the detection unit. Finally, the background estimation is selected by *VI* and *MR*, and the selected detectors are CA-CFAR, GO-CFAR and EESO-CFAR detectors. Select the corresponding detector for calculation, and finally multiply the corresponding threshold C_n and E_n to get *S*, and then get the final value compared with *D*. When $D \geq S$, the output H0; $D < S$, output H1, H0 indicates that the target is detected, H1 indicates that the detection is not the target.

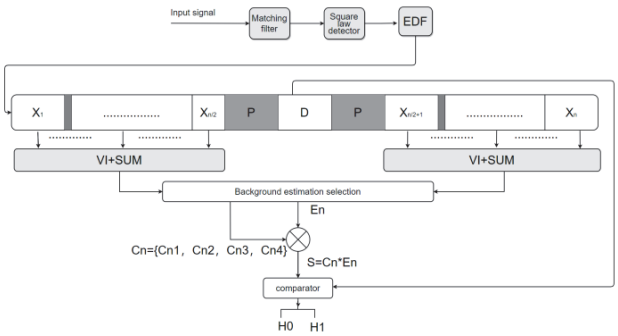

Figure 1 ESVI-CFAR detection principle flow diagram

EDF (Eliminate distractions first) represents the eliminating algorithm, and the schematic diagram is shown in Fig. 2. X_n represents all of the data. By dividing X_n into several small segments and sorting each segment, the KTH minimum value *M* is selected, and the detection unit larger than *M* is reserved to get *Y*.

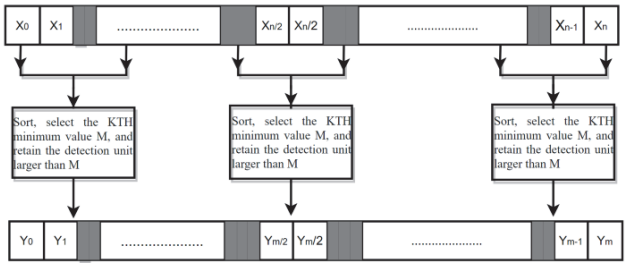

Figure 2 Flow chart of EDF filtering algorithm

Based on training data sets, EDF algorithm can eliminate non-target signals by learning and predicting the feature differences between target and non-target signals [28]. The basic process is as follows:

Collect training data. Training data sets containing target and non-target signals, and feature extraction of the data.

Build a classifier. Train the data set to build a classifier that classifies target and non-target signals.

Calculate the probability density function. Using the training data set, the probability density function of target and non-target signals is calculated (PDF). For each input signal, its probability score in the target and non-target PDF is calculated based on its eigenvector.

Calculate the *EDF* value. The *EDF* value of the input signal is calculated based on the probability scores of the target and non-target PDFS [29]. The *EDF* value can be calculated as follows:

$$EDF(x) = \frac{p(y=1|x)}{(p(y=1|x) + p(y=0|x))} \tag{1}$$

where, $p(y = 1|x)$ represents the probability that the input signal *x* belongs to the target class, and $p(y = 0|x)$ represents the probability that the input signal *x* belongs to the non-target class.

Identify and eliminate non-goals. According to the size of the *EDF* value, determine whether the input signal is the target. Under normal circumstances, a threshold is set, when the *EDF* value is greater than the threshold, the input signal is judged as the target, otherwise it is judged as a non-target.

1. The calculation of statistical variance *VI* is shown in Eq. (2) below.

$$VI = 1 + \frac{\tilde{\delta}^2}{\tilde{u}^2} = 1 + \frac{1}{\frac{n}{2} - 1} \sum_{i=1}^{\frac{n}{2}} \frac{(X_i - \bar{X})^2}{(\bar{X})^2} \tag{2}$$

In the expression, $\bar{X}$ represents the mean value of half a reference window; $\tilde{u}^2$ represents the estimated mean value of half a reference window; $\tilde{\delta}^2$ represents the variance estimate of half a window. X_i is the *i*-th data; *n* is the number of data; *i* is the data sequence number.

2. The ratio of the mean value of the front reference window to the mean value of the back reference window, *MR*, is calculated in the following Eq. (3):

$$MR = \frac{\bar{X}_A}{\bar{X}_B} = \frac{\sum_{i=1}^{\frac{n}{2}} X_i}{\sum_{i=\frac{n}{2}}^{n} X_i} \tag{3}$$

where, $\overline{X_A}$ and $\overline{X_B}$ respectively, represent the mean values of the pre-reference unit and post-reference unit of the detection unit.

After calculating the statistical variance *VI* and mean ratio *MR*, they are respectively compared with the statistical variance threshold *VK* and mean ratio threshold *MK*. The comparison results can indicate whether the clutter is uniform and whether the front and back reference Windows are approximately the same. The comparison formula and results are as follows:

When $VI \le VK$, uniform. If $VI > VK$, it indicates non-uniform.

When $MR^{-1} \le MR \le MK$, it means the mean is the same. When $MR^{-1} \ge MR$ or $MR \ge MK$, that means the mean is the same.

In the selection of background estimation, the corresponding threshold and detector can be selected by the above judgments. The threshold conditions and detector selection are shown in Tab. 1.

Table 1 ESVI-CFAR threshold calculation and detector selection

Frontier / *VI*	Back edge / *VI*	*MR*	Threshold calculation	CFAR Detector selection
$< VK$	$< VK$	$> MK^{-1}$ and $< MK$	$C_n * \frac{1}{n}\Sigma AB$	CA-CFAR
$< VK$	$< VK$	$< MK^{-1}$ or $> MK$	$C_n * \max\left(\frac{2}{n}\Sigma A, \frac{2}{n}\Sigma B\right)$	GO-CFAR
$> VK$	$< VK$	--	$C_n * \frac{2}{n}\Sigma B$	Rear reference window CA-CFAR
$< VK$	$> VK$	--	$C_n * \frac{2}{n}\Sigma A$	Rear reference window CA-CFAR
$> VK$	$> VK$	--	$C_n * \min\left(\frac{2}{n}\Sigma A, \frac{2}{n}\Sigma B\right)$	EESO-CFAR

In Tab. 1, *A* and *B* represent the front reference window and back reference window respectively, which are used in CA-CFAR, GO-CFAR and EESO-CFAR algorithms. CA-CFAR can achieve the best results under the background of uniform clutter. GO-CFAR detection has the best effect when the clutter is uniform but not level. In other cases, the EESO-CFAR detector discussed in this paper demonstrates good detection performance in practical applications.

3. Threshold factor selection under different detectors P_{fa} is assumed to be the false alarm probability, and the threshold factor of CA's clutter power estimation under a uniform clutter background is calculated as follows [30]:

$$C_n = (P_{fa})^{\frac{-1}{n}} - 1 \tag{4}$$

If the clutter background belongs to GO-CFAR, rear reference window CA-CFAR and front reference window CA-CFAR (rows 2 to 4 in Tab. 1), the threshold factor is calculated as follows:

$$C_n = (P_{fa})^{\frac{-1}{\frac{n}{2}}} - 1 \tag{5}$$

In the non-uniform environment along the reference window before and after processing, when *k* units are deleted from one of the reference window edges by comparing the reference units with the mean variance, the corresponding function (MGF) of local estimation generated is calculated as follows [31]:

$$P_{fa} = G_{xa}(x) = \binom{n}{k} \Pi_{j=1}^{k} [(n-k)C_n + \frac{N-j+1}{k-j+1}]^{-1} \tag{6}$$

In the formula, $G_{xa}(x)$ is Gamma function. Similarly, the local corresponding function MGF generated by another reference window edge after *h* units are deleted by mean variance is [32]:

$$M_b(u) = \binom{n}{h} \Pi_{j=1}^{h} [(n-h)C_n + \frac{N-j+1}{h-j+1}]^{-1} \tag{7}$$

Refer to *VI* & gt before and after. In the case of *VK*, it is only necessary to multiply the mean value of the side with the small mean value with C_n, and the result can be used as the final clutter power estimate.

3.2 ESVI-CFAR Implementation Method

1. Data processing

After calculating the statistical mean, identify the front and rear reference window edge; In the case of *VK*, the reference unit is divided into several segments, the number of reference units in each segment is k, and the mean value of *k* reference units in each segment is calculated.

Use the mean variance formula:

$$(X_i - \bar{X})^2 \le T \tag{8}$$

Remove the reference units that do not meet the requirements. If the mean variance is less than *T*, it means that the requirements are met. On the contrary, if the mean variance is greater than *T*, it means that the requirements are not met. Refer to Fig. 3.

Through the above experimental steps, calculate the mean *X* and *Y* of the remaining reference units, select the mean of the smaller reference units as E_n, and finally multiply the threshold factor C_n with E_n to wait until *S*. When *S* is compared with the target unit, it can determine whether the target information exists in the target unit. If it does, the output of the comparator will be H0; if it does not, the output of the comparator will be H1.

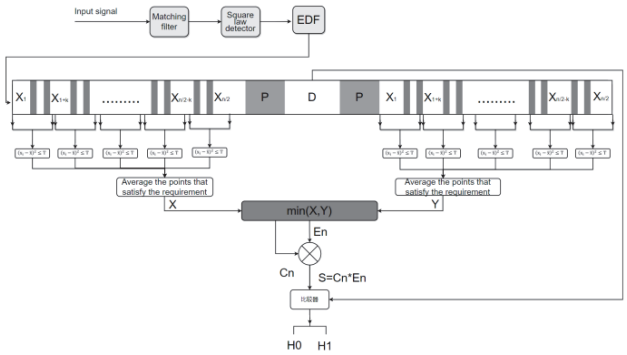

Figure 3 Schematic diagram of EESO-CFAR

2. Calculate the threshold parameter T

During the experiment, the target accuracy probability (P_d) and false alarm probability (P_{fa}) are both constants. When the value of T is larger, the system performance will be more unstable, and there will be interference with the target unit in the remaining reference unit, which will reduce the accuracy probability (P_d). On the contrary, the smaller the T value, most of the reference units will be excluded, making the performance of the detector approximate to CA-CFAR, and the clutter edge detection performance will be reduced, thus potentially increasing the probability of false alarm. Therefore, proper threshold parameter T is the key to the performance of the detector. This paper puts forward the formula of threshold T, which is as follows:

$$T = [(1 - P_{fa})^{(n-k)}](\bar{X})^2 \tag{9}$$

An appropriate threshold parameter T can be obtained through the above formula.

3. Grubbs criterion removes errors

The data is normalized in the experiment, i.e. the mean is subtracted and the standard deviation is divided, so that the data is distributed around the zero mean and the unit variance. Then the kernel density estimation function is used to smooth the normalized data so that it is closer to the true distribution. The accidental error is effectively eliminated, the accuracy and response speed are taken into account, and 13 times is taken as a unit. Among the 13 data obtained, some may contain large errors, which need to be sorted out, eliminate suspicious values, and improve the speed of self-adaptation. Calculate the G_i value: the residual/standard deviation of each data from the mean [33].

$$G_i = \frac{X_i - \bar{X}}{s} \tag{10}$$

Compare this G_i value with the critical value in the Grubbs critical table. The larger the value, the more abnormal it is.

4. Increase the negative sample

The optimal model uses the two-tower recall model to expand negative samples. The computational advantage of the two-tower model lies in the use of negative samples in batch samples to reduce the computational amount [34]. If we want to increase the number of samples in the batch, and increase the number of negative samples, we need more memory. Therefore, the authors propose a method to use previously trained data as a negative sample. When the neural network training reaches a certain number of rounds, stable vectors will be generated for the same samples. Therefore, when the previously trained data is used as the negative sample of the current training, the model only needs to take the vectors of these data and use them, and does not need to output new vectors to the neural network. The gap between the two vectors is small. This greatly reduces the amount of data to be processed and increases the processing time.

Expressed in $s(z, g)$ twin towers model calculation of similarity of user and item g z: $s(z, g) = \{u$ (z, the delta), v (g, the delta)$\}$. u represents the user tower, and the output user represents the vector; v is item, and the output item represents the vector. Finally, the similarity is the cosine of the two vectors. B represents a batch sample, and the formula for calculating the probability within the batch sample is [35]:

$$p_B(g_i \mid z_i; \delta) = \frac{e^{s(z_i, g_i)}}{\sum_{j \in [B]} e^{s(z_i, g_i)}} \tag{11}$$

FIFO (first in first out) queue is used, and the data tower output vector is put into the FIFO. When the training preparation reaches a certain number of rounds, a number of vectors are taken from the FIFO as vectors of negative samples when the model is trained. This not only reduces the amount of computation, but also reduces the memory usage when expanding negative samples.

4 ESVI-CFAR PERFORMANCE TEST

4.1 Accuracy and Reliability Verification of EDF

The total number of input data in the experiment is 2048, the *EDF* step size $S = 32$, $K = S/2 - n$. $S/2$), the target positions and numbers are random, and Monte Carlo simulation method was used to simulate the random waveform (including uniform clutter, uneven environment and clutter edge environment) for 10^6 times. The experimental results are shown in Tab. 2 (below) [23-27].

Table 2 Verification results of EDF in Monte Carlo simulation

Number of targets	n	*DNTU*	*DCNTU*	P_d
86	0	1026	83	96.51%
	5	1240	85	100.0%
	10	1843	86	100.0%
	15	2016	86	100.0%
342	0	1046	330	96.49%
	5	1368	339	99.12%
	10	1870	342	100.0%
	15	2013	342	100.0%
645	0	1046	582	90.23%
	5	1368	613	95.04%
	10	1870	640	99.22%
	15	2013	645	100.0%

Wherein, *DNTU* (detection is the number of target units) represents the number of target units detected by *EDF*. *DCNTU* (detection contains the number of target units) represents the number of targets detected by *EDF*, and P_d represents the accuracy in detecting targets. It can be seen from Tab. 2 that *EDF* has a higher screening level when $n = 10$.

4.2 Performance Analysis of ESVI-CFAR Detector

The ESVI-CFAR detector was simulated under the Monte Carlo simulation method. S = 32, n = 10 in EDF, false alarm probability $P_{fa} = 10^{-4}$ in ESVI-CFAR, statistical variance threshold VK = 4.76, statistical mean variance threshold MK = 1.806, number of reference units n = 32, number of protection units P = 2. On the premise of satisfying the above conditions, the Monte Carlo simulation was performed multiple times.

1. Test in a uniform clutter environment

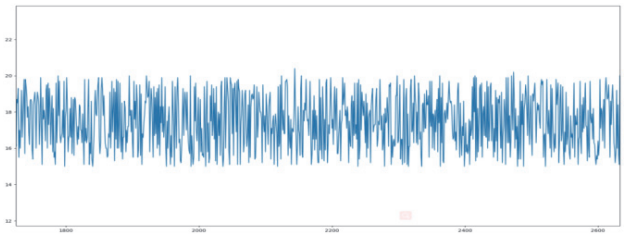

Figure 4 Uniform clutter diagram

Fig. 4 shows the uniform clutter diagram. As shown in the figure, the uniform clutter units follow an independent distribution, and the average power of the front and rear reference sliding windows of each target unit is similar ($VI < VK$ and $MR < MK$). Additionally, the figure does not contain any target cells.

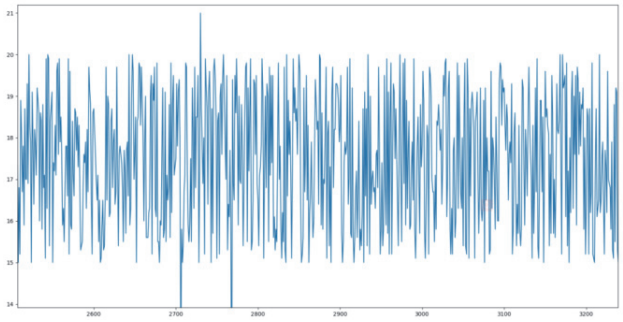

Figure 5 A uniform clutter pattern containing a target

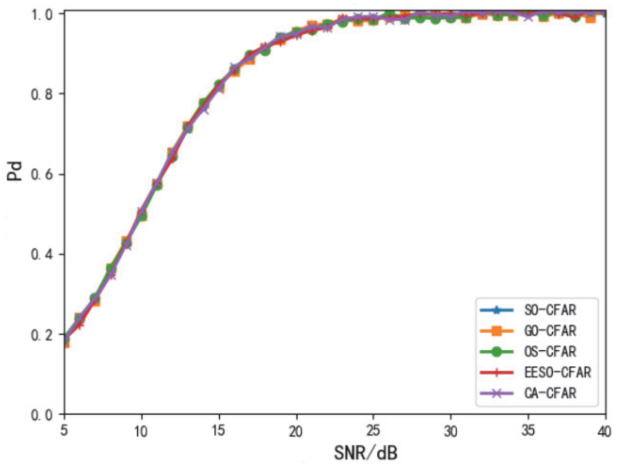

Figure 6 Performance of various detectors in a uniform environment

There is a target in a uniform background environment, and the power of the target is greater than most of the other reference units. The target's power reaches 21 dB. In the actual environment, the shape and size of the target seriously affect the power of the target, and different objects have different target power. When conducting CFAR, the accurate detection of the target becomes the standard to judge the performance of CFAR. For this reason, the results proved by the above conditional experiments are shown in Fig. 6.

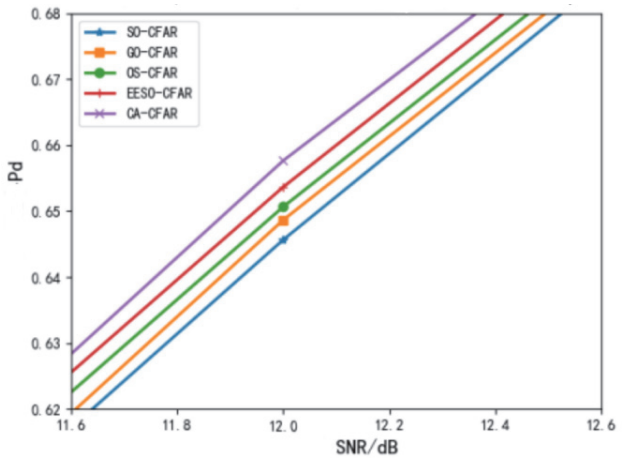

Figure 7 Local amplification performance of various detectors in a uniform environment

It is observed in Fig. 6 that the influence of target power on various detectors is almost the same in the environment of uniform clutter. When observed in Fig. 7, the detection performance of CA-CFAR is the best, followed by the EESO-CFAR mentioned in this paper, OS-CFAR, GO-CFAR and SO-CFAR.

2. Test in a multi-objective environment

In practical application, there are no interference units in the front and rear Windows of the reference units around the target (interference units: the units where other targets are located exist in this reference unit), and there are interference units in the half window interference units (interference units in the front window or reference units in the rear window) and in the front and rear Windows.

(1) There is no interference unit in front and rear Windows

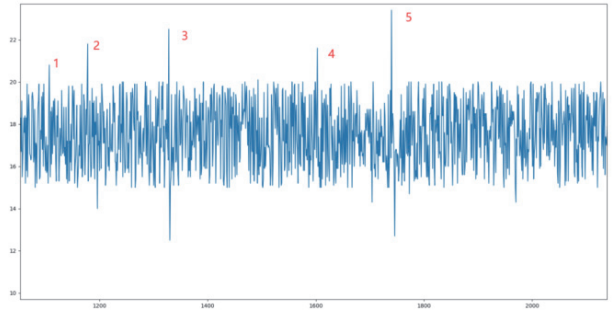

Figure 8 Uniform clutter diagram with multiple targets

By observing Fig. 8, we can see that there are 5 targets in the figure. The target units marked with ordered numbers are distributed in a uniform clutter environment, and there are no interference units in the front and rear window reference units ($VI < VK$, and $MR < MK$). This situation is the same as that of a target in a uniform environment, CA-CFAR still exhibits the best detection performance.

(2) Interference units exist in front or rear Windows

As can be seen from Fig. 9, there are eight targets with interference units along the reference window ($VIA > VK$ or $VIB > VK$, and $MR < MK$). Under the above conditions,

Monte Carlo simulation was conducted for several times, and the actual experimental data as shown in Fig. 10 were obtained in the near real environment.

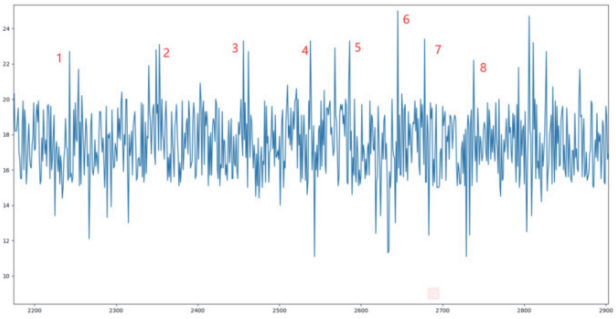

Figure 9 Multi-target one edge reference window with interference units

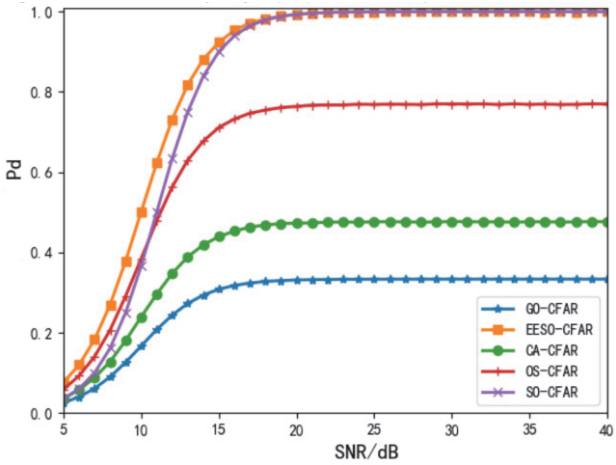

Figure 10 CFAR detection performance diagram with interference units

It can be clearly seen from the data in Fig. 10 that CA-CFAR and EESO-CFAR without interference cell edge have better performance. As can be seen from Fig. 11, CA-CFAR without interference cell edge has better effect.

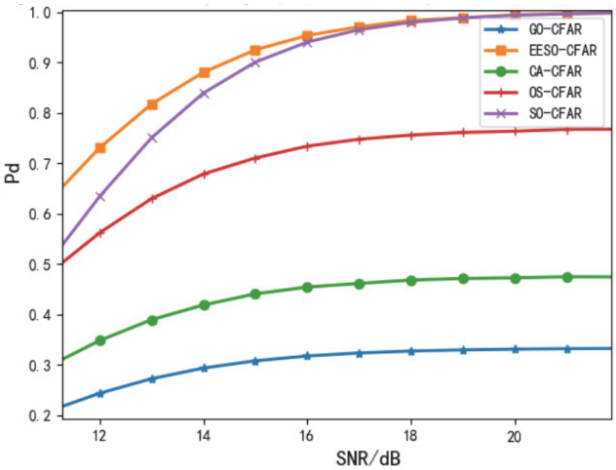

Figure 11 Enlarged view of CFAR detection performance with interference units

(3) Both front and rear Windows are tested with interference units (in non-uniform environment)

As can be seen from Fig. 12, there are three target units in the figure with non-uniform environments ($VI > VK$), there are interference units and clutter in the reference units of the front and rear Windows. Through various CFAR tests, the results are obtained as shown in Fig. 13.

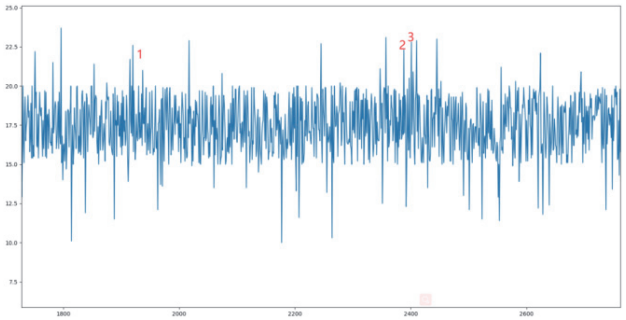

Figure 12 Multi-target in non-uniform environment

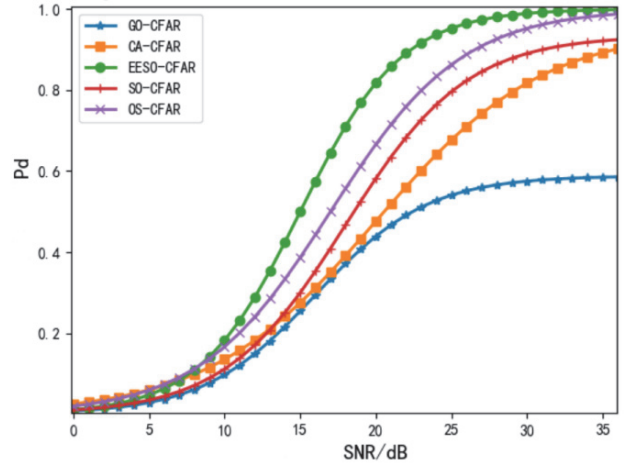

Figure 13 Multi-target non-uniform CFAR detection performance diagram

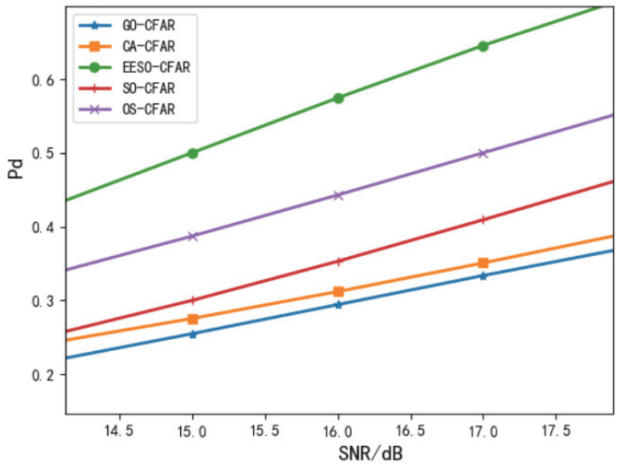

Figure 14 Local magnification of multi-target non-uniform CFAR detection performance

As can be seen from the experimental results in Fig. 13, the detection probability (P_d) of EESO-CFAR has obvious performance improvement compared with other CFAR detectors, followed by OS-CFAR detectors, SO-CFAR, CA-CFAR and GO-CFAR detectors have serious target loss and greatly reduced performance. In the process of CFAR detection, OS-CFAR detector also has good performance. In the detection, OS-CFAR only takes the KTH minimum value for reference comparison, but this will also make the reference value unstable, leading to the increase of false alarm probability. The EESO-CFAR detector can delete interference units and clutter, thereby reducing interference to the detection of target units and improving performance. This detector accurately detects the target and effectively reduces the probability of false alarms.

3. Test in clutter edge environment

In the clutter edge environment, there are homogeneous clutter edges ($VI < VK$, and $MR > MK$) and heterogeneous clutter edge environments ($VI > VK$, and $MR > MK$). Fig. 15 shows an example of a clutter edge environment.

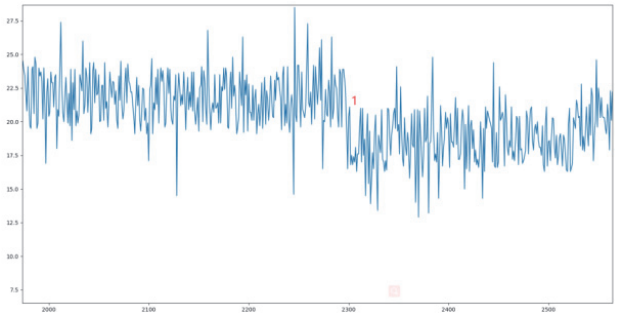

Figure 15 Clutter edge environment

(1) There are homogeneous clutter edges ($VI < VK$, and $MR > MK$)

During the experiment, various CFAR detectors were compared through the above environment. As can be seen from Fig. 16, GO-CFAR had the lowest probability of false alarm, followed by CA-CFAR with low probability of false alarm, and EESO-CFAR also better controlled the probability of false alarm. Compared with OS-CFAR, EESO-CFAR greatly reduced the probability of false alarm. The stability of the detector is improved.

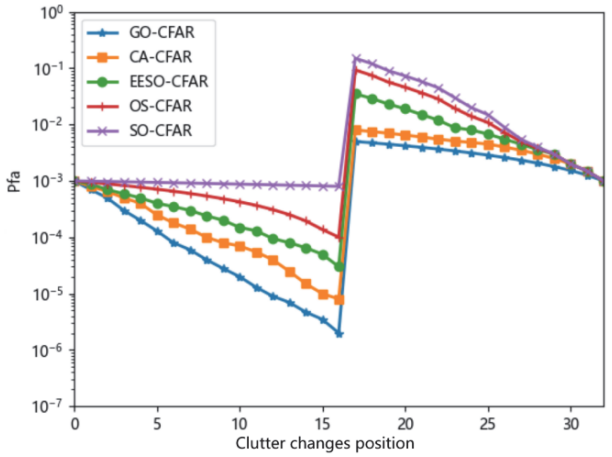

Figure 16 Performance diagram of CFAR detector in homogeneous clutter edge environment

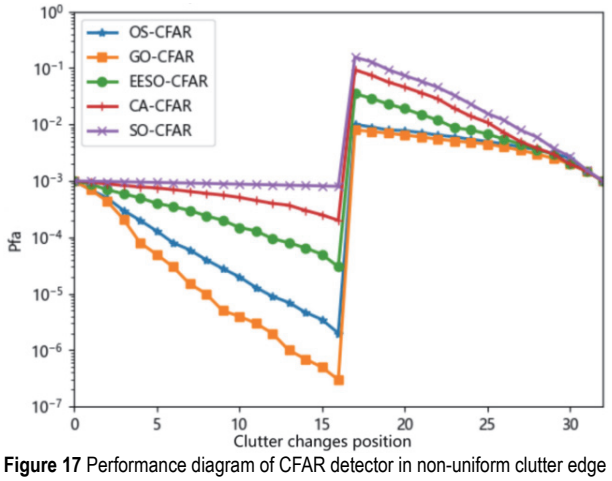

Figure 17 Performance diagram of CFAR detector in non-uniform clutter edge environment

(2) Inhomogeneous clutter edge environment (VI > VK, and MR > MK)

After the actual experiment, it can be seen from Fig. 17 that OS-CFAR is only sensitive to the KTH minimum value, and other reference units have no influence on it, leading to an increase of false alarm probability and greatly reduced detection performance of OS-CFAR. On the contrary, because the T in EESO-CFAR has adaptive ability, it will change the value of T according to the overall situation of the reference unit, so EESO-CFAR still maintains a high detection performance.

4.3 Speed Detection and Comparison of ESVI-CFAR

In the past VI-CFAR detection process, usually directly to the original data CFAR, which contains many non-target units. Due to the complexity of the VI-CFAR calculation process, all reference units required for VI-CFAR detection consume a lot of time and memory, so the ESVI-CFAR proposed in this paper can well solve the above problems. The EDF module in ESVI-CFAR has the ability to screen the target unit, greatly reducing the computing time and memory occupation. Experimental results are shown in Fig. 18 and Fig. 19 below.

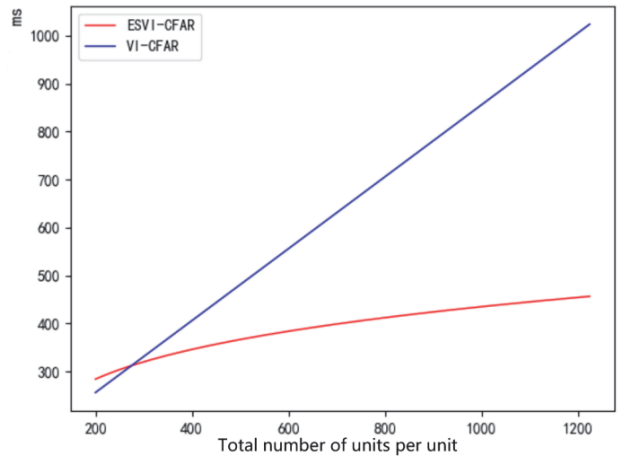

Figure 18 Relationship between the number of detection units of VI-CFAR and ESVI-CFAR and

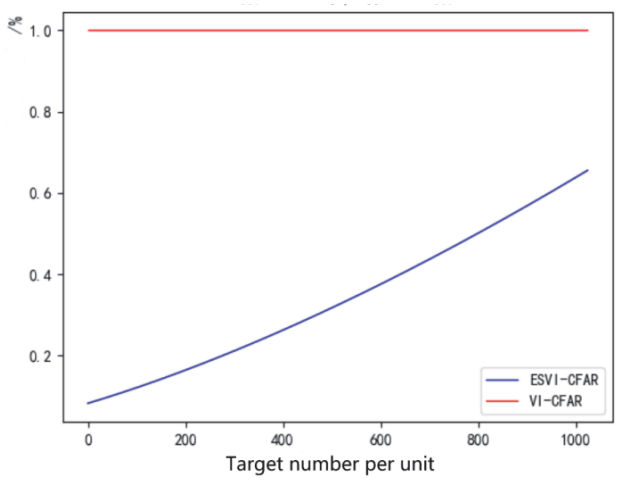

Figure 19 Relationship between the number of target units detected by VI-CFAR and ESVI-CFAR and time

As can be seen from Fig. 18 and Fig.19, when the number of targets is fixed at 100, the overall detection unit

increases and the detection consumption time of VI-CFAR increases linearly, while the detection consumption time of ESVI-CFAR increases with the increase of the number of targets, and the increase of the overall detection unit has little influence on ESVI-CFAR. When the number of units is 2048 and the number of targets is increased, the detection time of VI-CFAR reaches the maximum, while the detection time of ESVI-CFAR increases with the increase of targets. It can be seen that ESVI-CFAR has obvious advantages in terms of speed.

In the actual test, 150, 300, 500, 1000, 1200 unsigned fixed point numbers are taken as the target data input, and the reference window size N and protection window size M can be dynamically configured, where $1 \leq N \leq 27$, $1 \leq M \leq 17$, and N and M are odd numbers.

Table 3 ESVI-CFAR detector test

Input target number	Constant false alarm rate	Detection duration / ms	Signal-to-noise ratio boost / dB
150	71.28%	2.45	3.8
300	71.28%	2.47	3.8
500	71.29%	2.47	3.9
1000	71.30%	2.47	4.0
1200	71.30%	2.47	4.0

For ESVI-CFAR detectors, the detection was completed within 2.47 ms, and the constant false alarm probability was 71.3%. The signal-to-noise ratio is improved by about 4.0 dB. Compared with the test results of MATLAB software, the results are correct.

Tab. 4 shows the objective evaluation value of different detection methods. It can be seen that all algorithms have better values for those whose target values are prominent. For non-target values, the performance of all algorithms is degraded, but the algorithm in this paper still has a better value.

Table 4 Evaluation of detectors

Item	CA-CFAR	GO-CFAR	VI-CFAR	Textual algorithm
Detection duration / ms	$>$ 6.32	$>$ 6.58	$>$ 5.72	$<$ 2.47
Constant false alarm rate	63.30%	67.90%	69.20%	71.30%
Signal-to-noise ratio boost / dB	1.3	1.4	1.5	4.0

In general, the proposed algorithm has a certain robustness and can maintain a relatively stable detection rate for targets in different environments.

5 CONCLUSIONS

The optimized ESVI-CFAR detector eliminates the interference unit and clutter unit through reasonable acquisition threshold, so that the target detection is not disturbed, ensuring the detector has a high detection probability and reducing the false alarm probability. Using the pre-deletion mechanism (*EDF*), most of the non-target units can be deleted well, thus greatly reducing the processing time and memory consumption of the CFAR detector. This research contributes to the development of radar signal processing solutions for faster target detection, providing potential benefits for the sustainable development and utilization of high-performance radars.

Acknowledgements

Supported by Sichuan Science and Technology Program, China: 2023JDR0194.

6 REFERENCES

[1] Wang, P., Li, Q., Yin, P., Wang, Z., Ling, Y., Gravina, R., & Li, Y. (2023). A convolution neural network approach for fall detection based on adaptive channel selection of UWB radar signals. *Neural Computing and Applications*, *35*(22), 15967-15980. https://doi.org/10.1007/s00521-021-06795-w

[2] Giroux, J., Bouchard, M., & Laganiere, R. (2023). T-FFTRadNet: Object Detection with Swin Vision Transformers from Raw ADC Radar Signals. https://doi.org/10.48550/arXiv.2303.16940

[3] Ning, D. & Han, D. S. (2023). Radar Fault Detection via Camera-Radar Branches Learning Network. *2023 International Conference on Artificial Intelligence in Information and Communication (ICAIIC)*, 463-467. https://doi.org/10.1109/ICAIIC57133.2023.10067071

[4] Akhtar, J. (2023). High-Resolution Neural Network Processing of LFM Radar Pulses. *ICASSP 2023-2023 IEEE International Conference on Acoustics, Speech and Signal Processing (ICASSP)*, 1-5. https://doi.org/10.1109/ICASSP49357.2023.10095034.

[5] Zhou, J. & Xie, J. (2023). An Improved Quantile Estimator with its Application in CFAR Detection. *IEEE Geoscience and Remote Sensing Letters*. https://doi.org/10.1109/LGRS.2023.3309986

[6] Chen, Z., Chen, A., Liu, W., & Ma, X. (2023). CFAR Detection in Nonhomogeneous Weibull Sea Clutter for Skywave OTHR. *IEEE Geoscience and Remote Sensing Letters*. https://doi.org/10.1109/LGRS.2023.3313179

[7] Xu, M., Zhu, J., Fang, J., Zhang, N., & Xu, Z. (2023). CFAR based NOMP for Line Spectral Estimation and Detection. *IEEE Transactions on Aerospace and Electronic Systems*. https://doi.org/10.1109/TAES.2023.3282610.

[8] Zhang, W., Li, Y., Zheng, Z., Xu, L., & Wang, Z. (2023). Multi-Target CFAR Detection Method for HF Over-The-Horizon Radar Based on Target Sparse Constraint in Weibull Clutter Background. *Remote Sensing*, *15*(10), 2488. https://doi.org/10.3390/rs15102488

[9] Rosu, F. (2023). Dimension Compressed CFAR for Massive MIMO Radar. *IEEE Geoscience and Remote Sensing Letters*. https://doi.org/10.1109/LGRS.2023.3277713.

[10] Medeiros, D. S., García, F. D. A., Machado, R., Santos Filho, J. C. S., & Saotome, O. (2023). CA-CFAR Performance in K-Distributed Sea Clutter with Fully Correlated Texture. *IEEE Geoscience and Remote Sensing Letters*, *20*, 1-5. https://doi.org/10.1109/LGRS.2023.3238169.

[11] Ansila, V. M., Basheer, B., & Ambat, S. K. (2023). Computational Enhancement of Accumulated CA-CFAR Process in Side Scan Sonar Data. *2023 Sensor Signal Processing for Defence Conference (SSPD)*, 1-5. https://doi.org/10.1109/SSPD57945.2023.10256809.

[12] Uslu, A. & Ayazgök, S. (2023). Optimization of False Target Type Jamming Against CA-CFAR Utilizing Radars. *2023 31st Signal Processing and Communications Applications Conference (SIU)*, 1-4. https://doi.org/10.1109/SIU59756.2023.10224041

[13] Mboungam, A. H. M., Yongfeng, Z., & Youani, W. A. T. Moving Target Detection Using CA, SO and GO-CFAR detectors in Nonhomogeneous Environment. https://doi.org/10.5121/mathsj.2023.10202

[14] Mbouombouo Mboungam, A. H., Zhi, Y., & Youani, W. A. T. (2023). Moving Target Detection Using CA, SO and GO-

CFAR detectors in Nonhomogeneous Environment. *Applied Mathematics and Sciences: An International Journal (MathSJ), 7th International Conference on Applied Mathematics and Sciences (AMA 2023)*. https://doi.org/10.2139/ssrn.4453254

[15] Xiangwei, M. & Yuan, M. (2023). Modified rank sum nonparametric CFAR to combat clutter edge. *EURASIP Journal on Advances in Signal Processing*, *2023*(1), 75. https://doi.org/10.1186/s13634-023-01032-z.

[16] Baadeche, M. & Soltani, F. (2023). Closed-form expressions of PFA of mean level CFAR detectors for multiple-pulse gamma-distributed radar clutter. *Remote Sensing Letters*, *14*(10), 1056-1063. https://doi.org/10.1080/2150704X.2023.2264491

[17] Mboungam, A. H. M., Yongfeng, Z., & Youani, W. A. T. Moving Target Detection Using CA, SO and GO-CFAR detectors in Nonhomogeneous Environment. https://doi.org/10.5121/mathsj.2023.10202

[18] Liu, K., LI, Y., Wang, P., Peng, X., Liao, H., & Li, W. (2023). A CFAR Detection Algorithm Based on Clutter Knowledge for Cognitive Radar. *IEICE Transactions on Fundamentals of Electronics, Communications and Computer Sciences*, 106(3), 590-599. https://doi.org/10.1587/transfun.2022EAP1064

[19] Sim, Y., Heo, J., Jung, Y., Lee, S., & Jung, Y. (2023). FPGA Implementation of Efficient CFAR Algorithm for Radar Systems. *Sensors*, *23*(2), 954. https://doi.org/10.3390/s23020954

[20] Xiangwei, M. & Yuan, M. (2023). Modified rank sum nonparametric CFAR to combat clutter edge. EURASIP Journal on Advances in Signal Processing, 2023(1), 75.https://doi.org/10.1186/s13634-023-01032-z.

[21] Ahmad, Z., Nguyen, T. K., Rai, A., & Kim, J. M. (2023). Industrial fluid pipeline leak detection and localization based on a multiscale Mann-Whitney test and acoustic emission event tracking. *Mechanical Systems and Signal Processing*, *189*, 110067. https://doi.org/10.1016/j.ymssp.2022.110067

[22] Arumugam, R. K., Froehly, A., Herschel, R., Wallrath, P., & Pohl, N. (2023). Direction of Arrival Estimation on Sparse Arrays Using Compressive Sensing and MUSIC. *2023 17th European Conference on Antennas and Propagation (EuCAP)*, 1-5. https://doi.org/10.23919/EuCAP57121.2023.10133647

[23] Shen, L., Su, H., Mao, Z., Jing, X., & Jia, C. (2023). Signal Property Information-Based Target Detection with Dual-Output Neural Network in Complex Environments. *Sensors*, *23*(10), 4956. https://doi.org/10.3390/s23104956

[24] Zhang, Y. W., Ma, J. P., Zheng, H., & Gu, Z. (2023). Criticality-Aware EDF Scheduling for Constrained-Deadline Imprecise Mixed-Criticality Systems. *IEEE Transactions on Computer-Aided Design of Integrated Circuits and Systems*. https://doi.org/10.1109/TCAD.2023.3318512

[25] Eldele, E., Ragab, M., Chen, Z., Wu, M., Kwoh, C. K., Li, X., & Guan, C. (2023). Self-supervised contrastive representation learning for semi-supervised time-series classification. *IEEE Transactions on Pattern Analysis and Machine Intelligence*. https://doi.org/10.1109/TPAMI.2023.3308189

[26] Krause, I., Dantas, L. P., & Gimenez, S. P. (2023). Impact in the Parallel Processing of IHM-Plasma Using the Earliest-Deadline-First Algorithm for the Task-Scheduler Realized by Hardware. *Journal of Integrated Circuits and Systems*, *18*(1), 1-8. https://doi.org/10.29292/jics.v18i1.576

[27] Mangalampalli, S., Karri, G. R., Kumar, M., Khalaf, O. I., Romero, C. A. T., & Sahib, G. A. (2023). DRLBTSA: Deep reinforcement learning based task-scheduling algorithm in cloud computing. *Multimedia Tools and Applications*, 1-29. https://doi.org/10.1007/s11042-023-16008-2

[28] Li, J. & Zhou, X. (2023). YNUNLP at SemEval-2023 Task 2: The Pseudo Twin Tower Pre-training Model for Chinese Named Entity Recognition. *Proceedings of the 17th International Workshop on Semantic Evaluation (SemEval-2023)*, 1619-1624. https://doi.org/10.18653/v1/2023.semeval-1.224

[29] Zhu, Q. S., Zhou, L., Zhang, J., Liu, S. J., Hu, Y. C., & Dai, L. R. (2023). Robust data2vec: Noise-robust speech representation learning for asr by combining regression and improved contrastive learning. *ICASSP 2023-2023 IEEE International Conference on Acoustics, Speech and Signal Processing (ICASSP)*, 1-5. https://doi.org/10.1109/ICASSP49357.2023.10095373

[30] Feng, X., Dong, Z., Li, Y., Cheng, Q., Xin, Y., Lu, Q., & Xin, R. (2023). MSFC: a new feature construction method for accurate diagnosis of mass spectrometry data. *Scientific Reports*, *13*(1), 15694. https://doi.org/10.1038/s41598-023-42395-5

[31] Færch, L., Dierking, W., Hughes, N., & Doulgeris, A. P. (2023). A Comparison of CFAR Object Detection Algorithms for Iceberg Identification in L-and C-band SAR Imagery of the Labrador Sea. *The Cryosphere Discussions*, 1-26. https://doi.org/10.5194/tc-2023-17

[32] Sim, Y., Heo, J., Jung, Y., Lee, S., & Jung, Y. (2023). FPGA Implementation of Efficient CFAR Algorithm for Radar Systems. *Sensors*, *23*(2), 954. https://doi.org/10.3390/s23020954

[33] Giuffrida, L., Masera, G., & Martina, M. (2023). A Survey of Automotive Radar and Lidar Signal Processing and Architectures. *Chips*, *2*(4), 243-261. https://doi.org/10.3390/chips2040015.

[34] Zhang, H., Tian, M., Ouyang, Q., Liu, J., Shao, G., & Cheng, J. (2023). Track Detection of Underwater Moving Targets Based on CFAR. *Journal of Physics: Conference Series*, *2486*(1), 012076. https://doi.org/10.1088/1742-6596/2486/1/012076

[35] Feng, B., Gao, H., Yang, Y., Ren, F., & Lu, T. (2023). Multi-target CFAR detector based on compressed sensing radar system. *International Journal of Electronics*, 1-14. https://doi.org/10.1080/00207217.2023.2205170

Contact information:

Wei LI
(Corresponding author)
School of Electronic Information Engineering,
Geely University of China, Chengdu, 641423
E-mail: li.wei.77@163.com

Qian WANG
School of Electronic Information Engineering,
Geely University of China, Chengdu, 641423

Yuan-shuai LAN
School of Electronic Information Engineering,
Geely University of China, Chengdu, 641423

Chang-song MA
School of Electronic Information Engineering,
Geely University of China, Chengdu, 641423